J. Fluid Mech. (1970), *vol.* 43, *part* 3, *pp.* 497–511
Printed in Great Britain

Hypersonic viscous interaction on curved surfaces

By J. L. STOLLERY

Aerospace Research Laboratories, Wright–Patterson Air Force Base, Ohio†

(Received 9 December 1969)

Cheng's analysis of strong viscous interaction between a laminar boundary layer growing over a flat plate and the external hypersonic flow field is extended to cover curved surfaces. It is demonstrated that the solutions for some concave surfaces are oscillatory and quantitatively unrealistic. The reason for this behaviour is that the Busemann term in the Newton–Busemann pressure law used in Cheng's analysis over-corrects for centrifugal effects. The removal of the Busemann term or the substitution of the tangent-wedge pressure law results in an alternative analysis which can cover both strong and weak viscous interaction over a wide variety of two-dimensional shapes. A number of examples are included together with comparative experimental data.

1. Introduction

Laminar boundary-layer growth at hypersonic speeds can severely distort the external flow field, which in turn reacts to modify the boundary-layer growth. A good example of such viscous interaction is the flow near the leading edge of a flat plate where the boundary-layer growth gives rise to a strong, curved, oblique shock-wave followed by an expansion fan. The surface pressure distribution is then entirely different from the inviscid prediction. Rapid changes of boundary-layer growth will also occur in regions of strong pressure gradient, whether helpful or adverse, and in the design of any surface for high altitude hypersonic flight it is essential to predict the boundary-layer displacement thickness and hence the effective body shape with the modified pressure distribution that it supports.

The classic paper by Cheng *et al.* (1961) laid the foundations of the problem by clearly demonstrating the mutual effects of local surface incidence and boundary-layer growth. By adopting Lees' (1956) local flat plate similarity theory for hypersonic boundary layers, together with the Newton–Busemann approximation for the pressure distribution, Cheng was able to elegantly uncover the controlling parameter for strong viscous interaction over any shape of sharp edged surface, though the analysis was applied only to flat plates at incidence.

The use of the Newton–Busemann pressure law limited this work to regions of strong interaction but any one of a number of approximate pressure relations can be used in its place. More recently Sullivan (1969) has used the tangent-wedge approximation in combination with Lees' (1956) boundary-layer theory to investigate the flow around a convex corner.

† Permanent address: Aeronautics Department, Imperial College London.

The aim of this paper is to apply both Cheng's analysis, and modifications of it, to a wider variety of two-dimensional shapes, to compare and contrast the results and to discuss them in the light of experimental data wherever possible.

2. Analysis

The local flat plate similarity solution for hypersonic boundary layers leads to the following results (Prandtl number = 1):

$$\frac{M_\infty \delta^*}{x} = \tfrac{1}{2}(\gamma-1)\,0{\cdot}664\left(1+2{\cdot}6\frac{T_w}{T_0}\right)\bar{\chi}\left[\int_0^x \frac{p}{p_\infty}\frac{d\xi}{x}\right]^{\frac{1}{2}}\left(\frac{p}{p_\infty}\right)^{-1} \tag{1}$$

$$\equiv \frac{A\bar{\chi}}{P}\left[\int_0^x P\frac{d\xi}{x}\right]^{\frac{1}{2}},\dagger \tag{2}$$

$$M_\infty^3 St = 0{\cdot}332\,\bar{\chi}P\left[\int_0^x P\frac{d\xi}{x}\right]^{-\frac{1}{2}}, \tag{3}$$

and

$$C_f \simeq 2St, \tag{4}$$

where $\bar{\chi}$ is the viscous interaction parameter $M_\infty^3 C^{\frac{1}{2}}(Re_x)^{-\frac{1}{2}}$, St is the Stanton number, T_w and T_0 are the wall and stagnation temperatures respectively, P is the non-dimensional pressure distribution $p(x)/p_\infty$ and the other symbols are standard. Values of the constants for other Prandtl numbers have been quoted by Dewey (1963) and Sullivan (1968).

If the pressure distribution can be expressed in terms of the effective body shape, $y_e(x)$, as

$$P = P(y_e), \tag{5}$$

where

$$y_e = y_w + \delta^* \tag{6}$$

then (1), (5) and (6) can be solved for P, y_e and δ^* once the surface shape $y_w(x)$ is specified.

If the Newton–Busemann relation is used for the pressure distribution then

$$P = \gamma M_\infty^2(y_e'^2 + y_e y_e'') = \gamma M_\infty^2(y_e y_e')', \tag{7}$$

which, when substituted in (1), leads to the following result

$$(y_e - y_w)\{(y_e y_e')^{\frac{1}{2}}\}' = \left(\frac{A^2\bar{\chi}^2 x}{4\gamma M_\infty^4}\right)^{\frac{1}{2}}. \tag{8}$$

This is identical to Cheng's result apart from the minor change of γ now appearing in the denominator in place of unity. Equation (8) is the fundamental equation for y_e given any shape of wall and a number of examples will be considered. Since the right-hand side of (8) is constant it can be reduced to unity by appropriate scaling.

2.1. *Flat plate at zero incidence*

If $y_w = 0$ then writing

$$z = y_e/l \quad \text{and} \quad \zeta = x/l \tag{9}$$

† $A\bar{\chi}$ takes the place of $\bar{\chi}_\epsilon$ as used by Cheng *et al.* These two parameters differ only in that $\frac{1}{2}(\gamma-1)$ replaces $\epsilon \cong (\gamma-1)/(\gamma+1)$ in Cheng's theory. In the Newtonian approximation used by Cheng differences of order $\gamma-1$ are mathematically irrelevant.

converts equation (8) to
$$z((zz')^{\frac{1}{2}})' = 1, \tag{10}$$

provided that
$$l = \frac{A^2\bar{\chi}^2 x}{4\gamma M_\infty^4}. \tag{11}$$

Substitution of $z = k\zeta^m$ in equation (10) shows that it is satisfied for $m = \frac{3}{4}$ and $k = 2^{\frac{3}{2}}/3^{\frac{1}{4}}$ yielding the familiar strong interaction results:

$$\frac{M_\infty \delta^*}{x} = \frac{2}{(3\gamma)^{\frac{1}{4}}}(A\bar{\chi})^{\frac{1}{2}}, \tag{12}$$

$$P = (\tfrac{3}{4}\gamma)^{\frac{1}{2}} A\bar{\chi}, \tag{13}$$

and
$$St/St_0 = \tfrac{1}{2}(3\gamma)^{\frac{1}{4}}.(A\bar{\chi})^{\frac{1}{2}}, \tag{14}$$

where St_0, the Stanton number for a flat plate flow with no viscous interaction, is given by
$$St_0 = 0{\cdot}332(C/Re_x)^{\frac{1}{2}}. \tag{15}$$

The weak viscous interaction solution where $P \to 1$ as $y_e' \to 0$ does not satisfy the Newton–Busemann relation and hence is not a solution of equation (10).

2.2. *Surfaces described by* $y_w = kx^n$

The family of shapes
$$\frac{y_w}{\alpha l} = \pm\left(\frac{x}{l}\right)^n \quad \text{or} \quad z = \pm\zeta^n, \tag{16}$$

is of some interest and includes the flat plate at incidence, ($n = \pm 1$). The governing equation may now be written as

$$(z \mp \zeta^n)\,((zz')^{\frac{1}{2}})' = 1, \tag{17}$$

provided that
$$l = \frac{A^2\bar{\chi}^2 x}{4\gamma M_\infty^4 \alpha^4}. \tag{18}$$

In terms of the new variables the required physical quantities are

$$\frac{\delta^*}{\alpha l} = (z \mp \zeta^n), \tag{19}$$

$$\frac{P}{\gamma M_\infty^2 \alpha^2} = (zz')', \tag{20}$$

and
$$\frac{A\,St}{0{\cdot}332\alpha^3 4\gamma} = \frac{1}{(z \mp \zeta^n)} = \left(\frac{\delta^*}{\alpha l}\right)^{-1}. \tag{21}$$

Thus from the scaling it is immediately apparent that the important parameter which controls the relative importance of the effects of incidence and strong viscous interaction is $(M_\infty^2\alpha^2/A\bar{\chi})$.

2.3 *Alternative expressions for the pressure law,* $P(y_e)$

The scope of the theoretical analysis can be extended by using an alternative pressure law which is capable of embracing both the strong and weak viscous

interaction régimes. For example a simple Newtonian law could be used in the form

$$P \equiv p/p_\infty = 1+\gamma M_\infty^2 y_e'^2 \equiv 1+\gamma K^2, \tag{22}$$

where

$$K = M_\infty y_e', \tag{23}$$

so that P in the free-stream is interpreted as unity rather than zero. One of the more successful approximations at hypersonic speeds is the tangent wedge rule,

$$P = 1+\gamma K^2\left[\frac{\gamma+1}{4}+\left\{\left(\frac{\gamma+1}{4}\right)^2+\frac{1}{K^2}\right\}^{\frac{1}{2}}\right], \tag{24}$$

and Sullivan (1969) has used this in place of the Newton–Busemann law to examine flow past a convex corner. Though the use of either of the above pressure relationships decreases the mathematical elegance there is a great gain in practical utility and the subsequent analysis is straightforward.

The boundary-layer growth may be expressed (see equation (1)) as

$$\frac{M_\infty \delta^*}{L} = A\bar{\chi}\left(\frac{x}{L}\right)^{\frac{1}{2}}\cdot\frac{R^{\frac{1}{2}}}{P} \tag{25}$$

and if L, a characteristic length, is chosen such that

$$L = A^2\bar{\chi}^2 x, \tag{26}$$

then

$$X = x/L = (A\bar{\chi})^{-2} \tag{27}$$

and

$$M_\infty \delta^*/L = R^{\frac{1}{2}}/P, \tag{28}$$

where

$$dR/dX = P. \tag{29}$$

Equation (28) may be differentiated to give

$$\frac{M_\infty d\delta^*}{dx} = \frac{1}{2R^{\frac{1}{2}}} - \frac{R^{\frac{1}{2}}}{P^2}\cdot\frac{dP}{dX}, \tag{30}$$

and $d\delta^*/dx$ may be expressed in terms of P from either of the pressure laws. The result for a family of shapes

$$Y_w = X^n, \tag{31}$$

where $Y_w = y_w/\alpha L$ and $X = x/L$, is

$$\frac{dP}{dX} = \frac{P^2}{2R}\left\{1+2R^{\frac{1}{2}}\left[M_\infty \alpha \frac{dY_w}{dX} - Q\right]\right\}, \tag{32}$$

$$\frac{dR}{dX} = P, \tag{33}$$

where

$$Q = \frac{P-1}{\gamma\left\{1+\frac{\gamma+1}{2\gamma}(P-1)\right\}^{\frac{1}{2}}} \quad \text{for the tangent wedge rule}$$

and

$$= \left(\frac{P-1}{\gamma}\right)^{\frac{1}{2}} \quad \text{for the Newtonian pressure distribution.}$$

The analysis underlines the importance of $M_\infty \alpha$ and $A\bar{\chi}$ as the relevant parameters but they must now be specified independently for solutions of the pair of equations (32) and (33).

Once $M_\infty \alpha$ is specified then the equation pair may be solved for any given shape. For example the substitution of $\alpha = 0$ (flat plate at zero incidence) and $P = kX^m$ with $P \gg 1$ enables k and m to be evaluated so that

$$P = \tfrac{3}{4}[\gamma(\gamma+1)]^{\frac{1}{2}}.A\overline{\chi} \quad \text{(tangent wedge)} \tag{34}$$

or

$$P = \tfrac{3}{2}(\tfrac{1}{2}\gamma)^{\frac{1}{2}}.A\overline{\chi} \quad \text{(Newtonian)}, \tag{35}$$

is the appropriate result for strong viscous interaction. The weak viscous interaction condition is also satisfied since

$$\frac{dP}{dX} \to \frac{1}{2X} \quad \text{as} \quad P \to 1, \quad \text{i.e.} \frac{dP}{dX} \to 0 \quad \text{as} \quad X \to \infty.$$

3. Results, comparisons with experimental data and discussion

The governing equations for both Cheng's and the modified theories have been solved for a variety of surfaces including the flat plate at both positive and negative incidence, concave and convex plates ($n = 2, 3$) and compression and expansion corners. The numerical results were obtained by digital computation using an IBM 7094 machine and Fortran IV language. A standard third-order Runge–Kutta technique was adopted with double precision arithmetic and a step size of usually 10^{-4}.

3.1. *Flat plate at zero incidence*

Comparisons between the various theories and some experimental data are shown in figures 1 and 2. Cheng's theory is strictly for strong interaction only, though it can be used more widely if the calculated pressure distribution is interpreted as $(P - P_{x=\infty})$. Either way the theory immediately highlights the importance of the parameter $A\overline{\chi}$. The use of the tangent-wedge rule for pressure gives a smooth

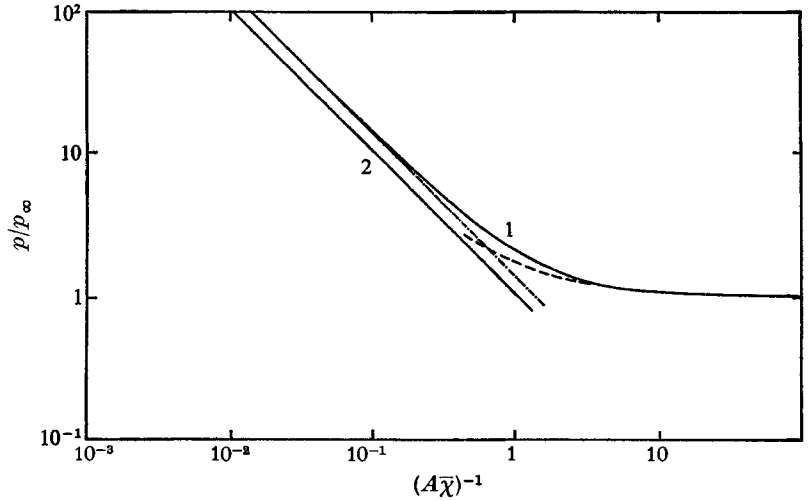

FIGURE 1. A comparison between various theoretical estimates of the pressure distribution induced on a sharp flat plate at zero incidence. —— 1, complete solution (Sullivan); —— 2, Cheng's theory, $p/p_\infty = (\frac{3}{4}\gamma)^{\frac{1}{2}}A\overline{\chi}$; - - - -, weak interaction theory $p/p_\infty = 1 + \frac{1}{2}\gamma A\overline{\chi}$; –·–·–, strong interaction theory.

transition from strong to weak interaction, as shown by Sullivan (1969). Figure 2 suggests that Sullivan's theory predicts the Stanton number reasonably accurately but overestimates the pressure level. The scatter in the experimental pressure data is due partly to low density effects.

3.2. *Flat plate at incidence*

The pressure distribution over a flat plate at positive incidence (i.e. nose down) as calculated using the methods of Cheng and Sullivan is shown in figure 3. The results indicate that near the leading edge the displacement effect is

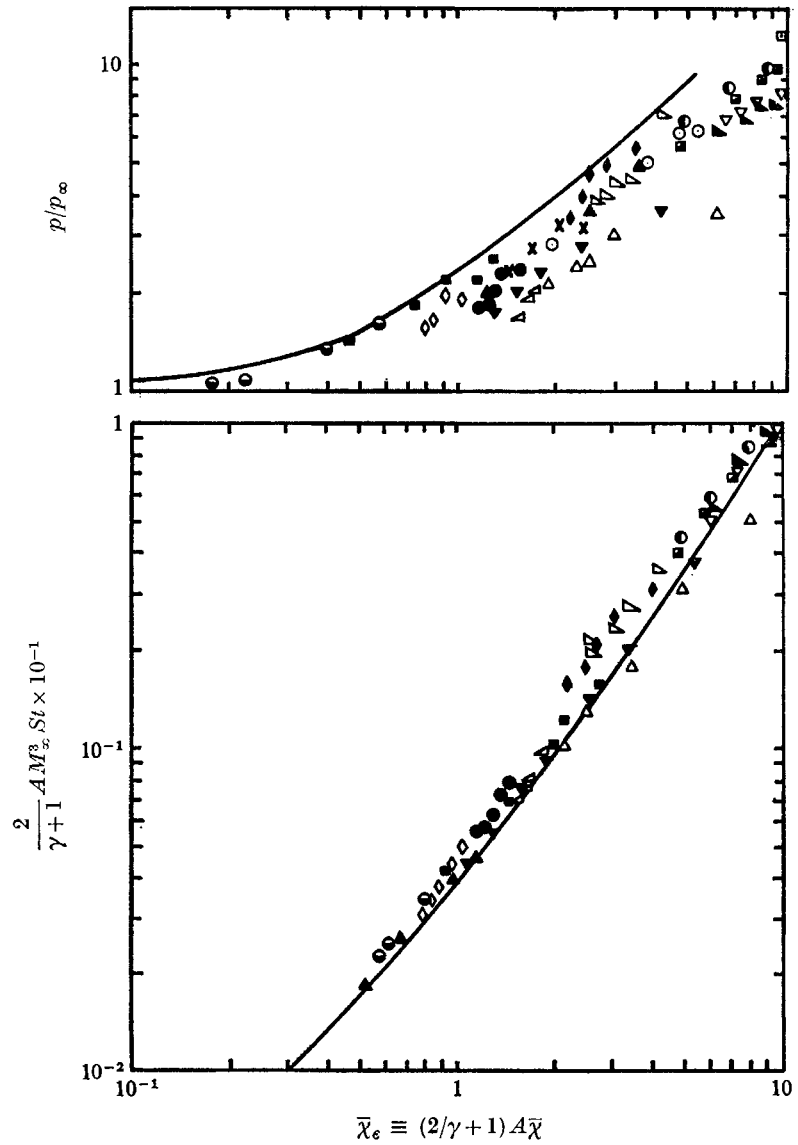

FIGURE 2. Correlation of pressure and heat transfer data on sharp flat plates. ——, theory, $Pr = 1$. Data for both diagrams taken from Holden (1970).

dominant and the pressure distribution is identical to that on a flat plate at zero incidence. Further downstream the incidence effects increase in importance and eventually the pressure level asymptotes to the inviscid limit.

Cheng's theory holds for all values of $M\alpha$ provided that the shock is strong. Kemp (1969) has recently reported some tests in helium at $M = 42$ which show that Cheng's theory predicts the trends quite well under these conditions.

If the tangent-wedge approximation is used then there is a different solution for every value of $M\alpha$ and the asymptotic pressure level is

$$\frac{P}{\gamma M_\infty^2 \alpha^2} = \left\{\frac{\gamma+1}{4} + \left[\left(\frac{\gamma+1}{4}\right)^2 + \frac{1}{M_\infty^2\alpha^2}\right]^{\frac{1}{2}}\right\} + \frac{1}{\gamma M_\infty^2 \alpha^2}. \tag{36}$$

This will only approach Cheng's value of unity when $M_\infty \alpha \gg 1$ and $\gamma = 1$. Because of these differing asymptotes the curves look dissimilar. A more realistic comparison can be achieved either by interpreting Cheng's result as $P - P_{\text{wedge}}$ so that his asymptotic value becomes

$$P_{\text{wedge}} = 1 + \gamma M^2 \alpha^2,$$

or by plotting all the results as

$$\frac{P - P_{\text{wedge}}}{\gamma M^2 \alpha^2} + 1.$$

Presented in this way the curves compare well, see figure 4(*a*).

The heat transfer rates calculated by the two methods are similar, figure 4(*b*), the agreement improving as $M\alpha$ is increased. Cheng's results show that it is not until $M^2\alpha^2/A\bar{\chi}$ is of order unity that large deviations from the zero incidence condition occur. Cheng's zero incidence flat plate value for the Stanton number may be conveniently expressed as

$$\frac{A\,.\,St}{0{\cdot}332 \times 4\gamma\alpha^3} = \frac{(3\gamma)^{\frac{1}{2}}}{8\gamma} \cdot \left\{\frac{M^2\alpha^2}{A\bar{\chi}}\right\}^{-\frac{1}{2}}. \tag{37}$$

Similar remarks apply to the negative incidence results. Any calculations made using Cheng's method must show the pressure distribution tending asymptotically to zero whereas the tangent wedge limit is given by

$$P = 1 + \gamma M^2 \alpha^2 \left\{\frac{\gamma+1}{4} - \left[\left(\frac{\gamma+1}{4}\right)^2 + \frac{1}{M_\infty^2\alpha^2}\right]^{\frac{1}{2}}\right\}. \tag{38}$$

Since P cannot be negative the lowest permissible value of $M\alpha$ is $-[2/\gamma(\gamma-1)]^{\frac{1}{2}}$. Of course the range of the calculations could be extended by using a more suitable pressure law for expanding flows.

3.3. *Concave surfaces*: $Y_w = X^n$ $(n = 2, 3)$

The most striking feature of the results obtained by applying Cheng's theory to these shapes is the 'oscillatory' behaviour of the boundary layer.† The boundary layer, dominated near the leading edge by displacement effects, grows initially

† The theoretical asymptotic behaviour of equation (17) has been investigated by Mohammadian (private communication) and found to be oscillatory for concave surfaces of the form $y = kx^n$ provided that $n > 1$. Similar oscillatory behaviour has been noted by Cheng & Kirsch (1969) in their recent study of intense explosions.

as though supported by a flat plate. Faced with the adverse pressure gradient downstream the boundary layer thins dramatically to a 'neck' then widens again and the cycle of events is then repeated. Beneath each 'neck' the pressure and heat transfer rate reach local peaks. This pattern of behaviour is similar in character but much more severe in magnitude to that found experimentally and it appears that the Busemann centrifugal correction is far too powerful in the assumed pressure law. As the flow moves around the surface the dominant

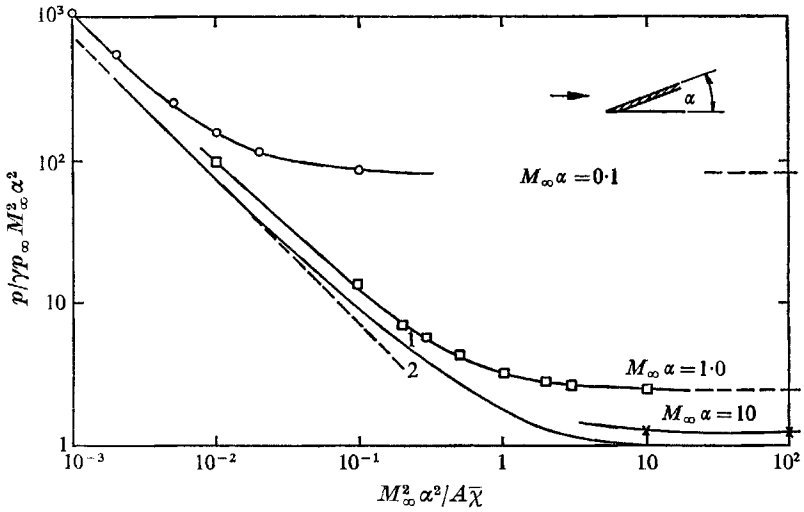

FIGURE 3. Predictions of the pressure distribution on a flat plate at positive incidence. —— 1, Cheng; – – – 2, strong viscous interaction, flat plate at $\alpha = 0$.

influence changes from displacement to incidence and the pressure should approach the inviscid value,

$$P = \gamma M_\infty^2 (Y_w Y_w')'. \tag{39}$$

For $n = 2$ ($Y_w = X^2$) this relationship implies that

$$\frac{P}{\gamma M^2\alpha^2} = 6X^2 = 96\gamma^2\left\{\frac{M^2\alpha^2}{A\bar{\chi}}\right\}^4 \tag{40}$$

and, as figure 5 shows, the pressure distribution does in fact oscillate about this line for X large.

Similar remarks apply to the cubic surface, the downstream pressure levels oscillating about the curve

$$\frac{P}{\gamma M^2\alpha^2} = 15X^4 = 3840\gamma^4\left\{\frac{M^2\alpha^2}{A\bar{\chi}}\right\}^8. \tag{41}$$

When the more realistic tangent-wedge approximation is used then there is no oscillation, the boundary-layer thickness decreasing steadily as the pressure rises. As a further check the modified Newtonian pressure distribution,

$$P = 1 + \gamma K^2,$$

was used to calculate the flow around the quadratic surface and the result is also plotted on figure 5. There is no oscillatory behaviour and the numerical values are close to those calculated using the tangent-wedge law.

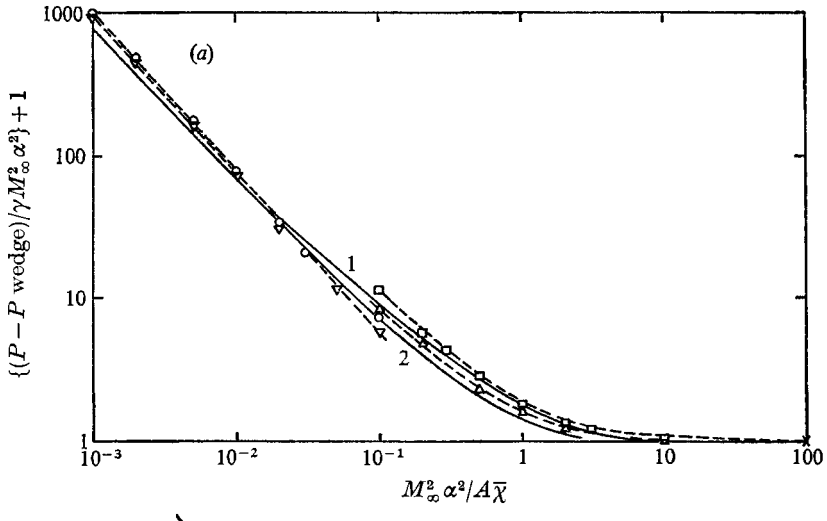

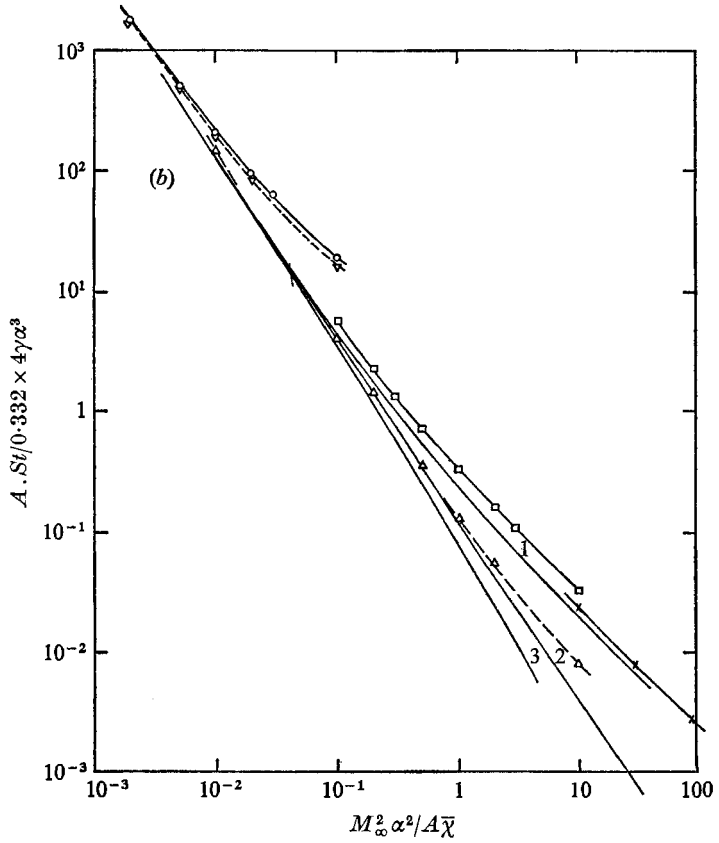

FIGURE 4(*a*). Pressure distribution on flat plates at positive and negative incidence. —— 1, Cheng, $\alpha > 0$; —— 2, Cheng, $\alpha < 0$. Complete solutions using the tangent-wedge rule, values of $M_\infty\alpha$: ○, 0·1; □, 1·0; ×, 10; ▽, −0·1; △, −1·0.

FIGURE 4(*b*). Heat transfer to a flat plate at positive and negative incidence. —— 1, Cheng, $\alpha > 0$; —— 2, Cheng, $\alpha = 0$; —— 3, Cheng, $\alpha < 0$. $M_\infty\alpha$: ○, 0·1; □, 1·0; ▽, −0·1; △, −1·0; ×, 10.

Figure 6 shows the heat transfer rate distributions for the body $y_w = kx^2$. Values calculated using Cheng's method oscillate about the limiting value which for this shape of body is

$$\frac{A.St}{0{\cdot}332 \times 4\gamma.\alpha^3} = (6(\tfrac{1}{2}\gamma)^{\frac{1}{2}})\left(\frac{M^2\alpha^2}{A\bar{\chi}}\right). \tag{42}$$

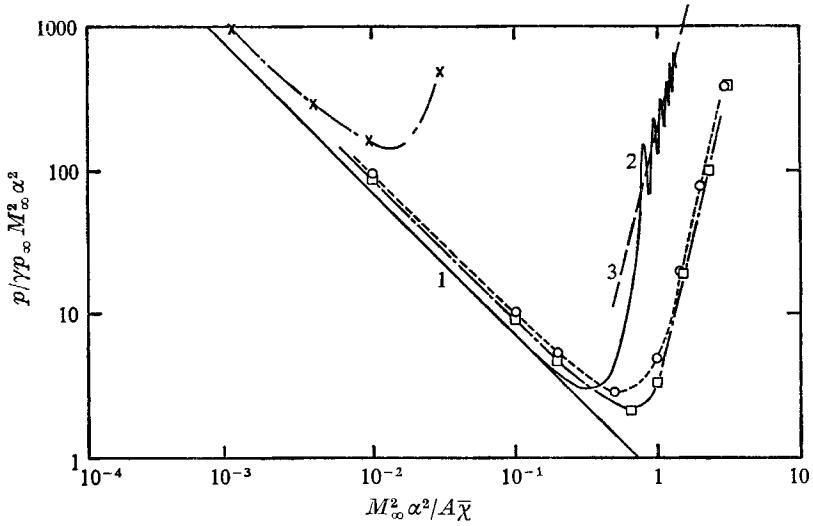

FIGURE 5. The pressure distribution on a concave surface of the form $y_w = kx^2$. —— 1, strong interaction, flat plate at $\alpha = 0$; —— 2, Cheng's theory; – – 3, $96\,\gamma^2\{M_\infty^2\alpha^2/A\bar{\chi}\}^4$. Tangent wedge, $M_\infty\alpha$: ×, 0·1; ○, 1·0. $p_e/p_\infty = 1+\gamma M_\infty^2 y_e'^2$, $M_\infty\alpha$: □, 1·0.

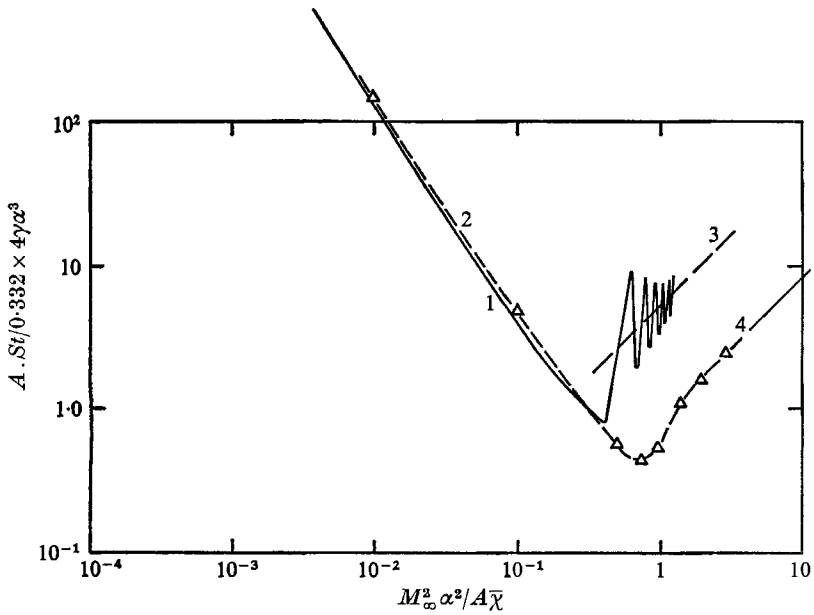

FIGURE 6. The heat transfer to a concave surface of the form $y_w = kx^2$. —— 1, Cheng's theory; – – – 2, solution using tangent-wedge rule, $M_\infty\alpha = 1$; – – – 3, $6(\frac{1}{2}\gamma)^{\frac{1}{2}}M_\infty^2\alpha^2/A\bar{\chi}$; – — 4, asymptotic value, $y_e = y_w$.

In contrast the values calculated using either the tangent-wedge or modified Newtonian pressure laws are well behaved, approach the asymptotic value smoothly and are physically more realistic.

Two theoretical predictions of boundary-layer growth over a cubic surface ($y_w = x^3/150$) are compared with an estimate made from a schlieren picture of the flow in figure 7. The 'pulsating' thickness predicted by Cheng's method is clearly shown with the outer edge coming very close to the wall at the first 'neck'. The estimate using the tangent-wedge law is more realistic with the layer thinning slowly but continuously in the downstream region.

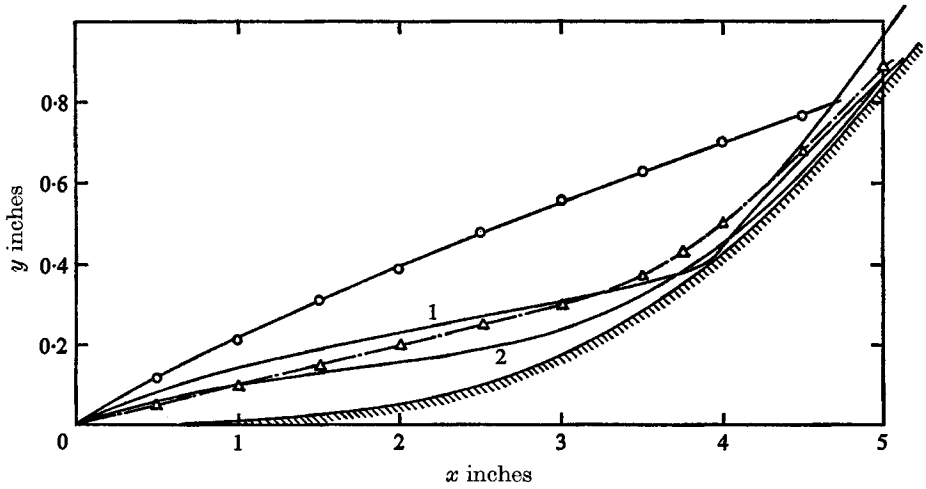

FIGURE 7. Boundary-layer growth over a cubic concave body, ($y_w = x^3/150$, where x and y_w are in inches). —— 1, δ^* Newton–Busemann pressure law; —— 2, δ^* tangent-wedge rule; —○—, shock position from photograph; —△—, 'edge' of boundary layer as measured from schlieren photograph.

Both estimates describe broadly the main features of the flow. Near the leading edge the displacement effect is dominant and the layer grows much as it would over a flat plate. Then as the surface slope increases so the incidence effect grows in importance and the slope of the outer edge of the layer approaches that of the wall. The approximate estimate of boundary-layer thickness taken from a schlieren picture confirms these trends. The favourable comparison between the measured pressure distribution along the cubic surface and an estimate made using the tangent-wedge rule is shown in figure 8.

3.4. *Convex surfaces*

For convex surfaces Cheng's method does not give oscillatory answers, the boundary layer growing rapidly but smoothly in the helpful pressure gradient. Since the Newton–Busemann law is used the theory can only apply if y'_e is positive, i.e. in regions close to the leading edge or where the negative body slope is small. Figure 9 compares the pressure distribution over three surfaces of the family $Y = -X^n$ where $n = 1$, 2 and 3.

3.5. *Flow past compression corners*

As now expected Cheng's method predicts an oscillatory behaviour more violent than that found experimentally. Therefore, only the method suggested by Sullivan has been used to compare some theoretical predictions with experimental

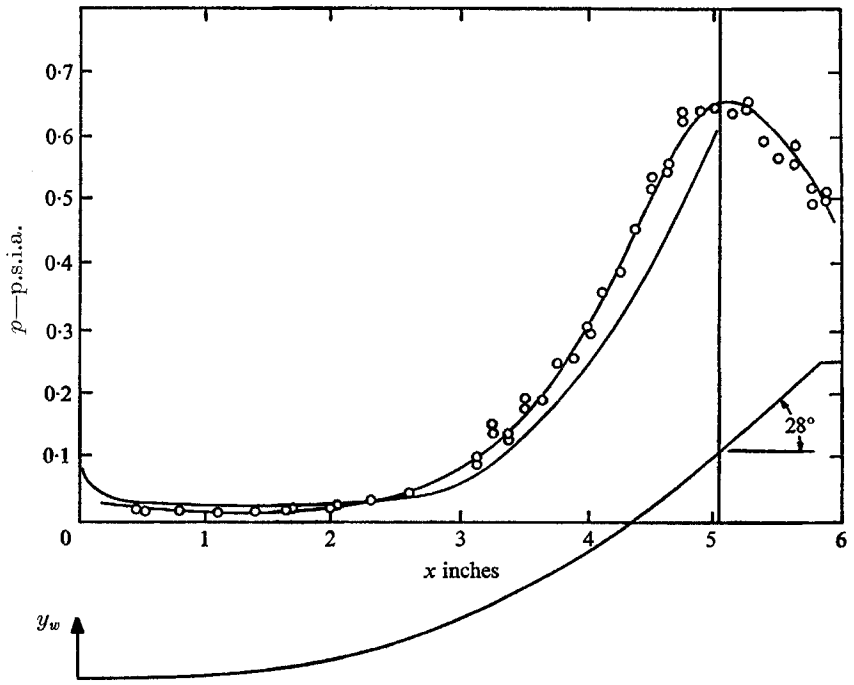

FIGURE 8. Pressure distribution on a concave cubic body. $y_w = x^3/150$ where x and y_w are in inches and $0 < x \leqslant 5{\cdot}1$. ——, theory; —○—, measurements, $M_\infty = 12{\cdot}25$, $Re = 0{\cdot}86 \times 10^5$ per inch.

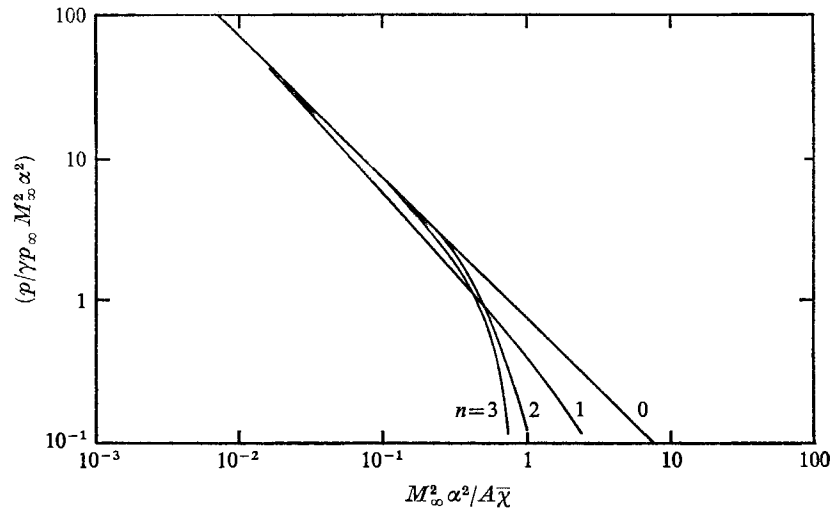

FIGURE 9. Theoretical pressure distribution on convex surfaces of the form $y_w = kx^n$; $n = 0$, 1, 2 and 3.

data. Comparisons have been made with three sets of pressure and heat transfer rate data at $M = 9{\cdot}7$ and 20 (figures 10(*a*)–(*c*)). Considering the simplicity of the mathematical model and the closeness of the experimental flows to incipient separation the agreement between prediction and measurement is encouraging.

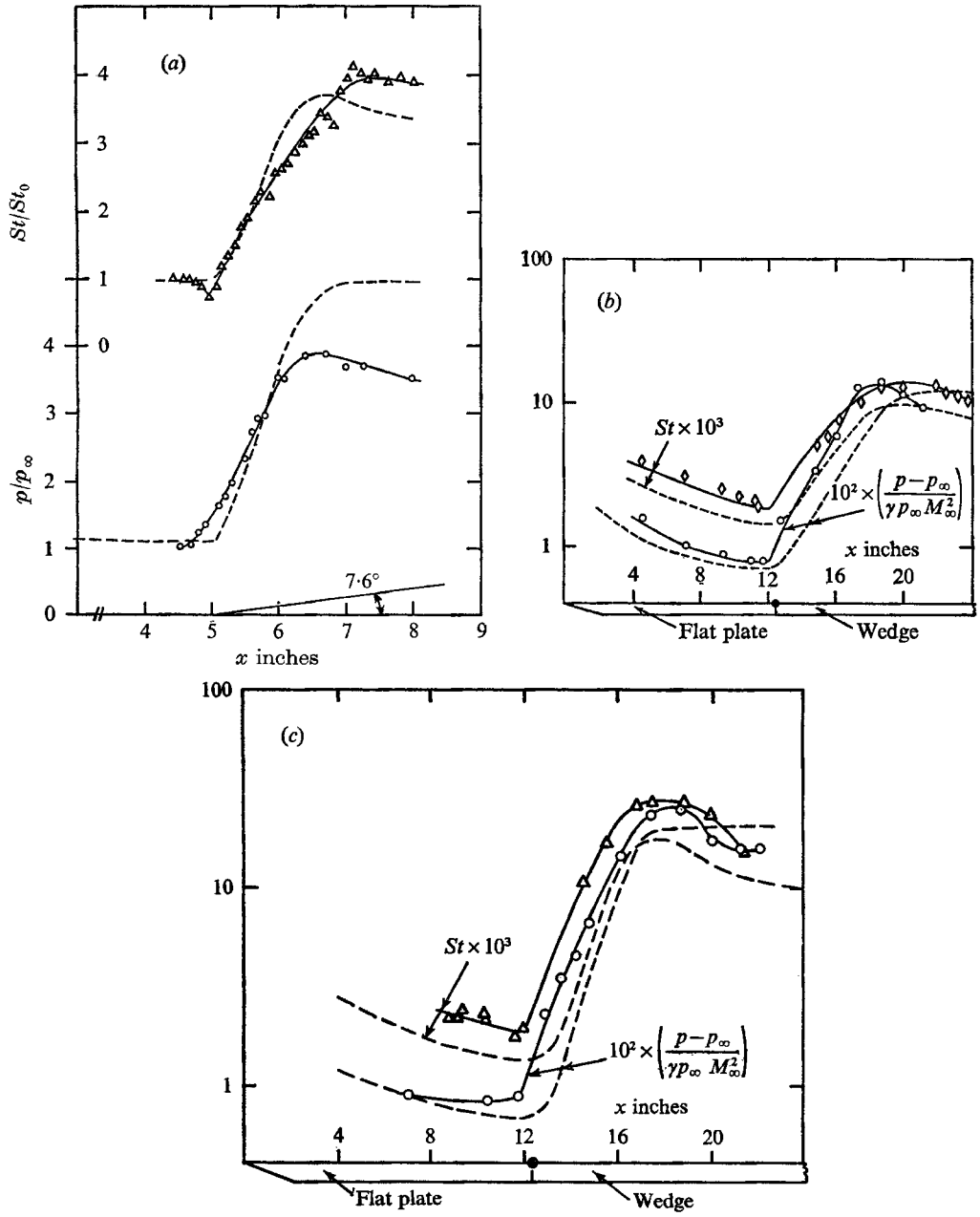

FIGURE 10. Comparisons between the theoretical and experimental distributions of pressure and heat transfer rate on a compression corner model. – – –, theory; —○—, —△—, —◇—, measurements. (*a*) $M_\infty = 9{\cdot}7$, $\alpha_{\text{wedge}} = 7{\cdot}7°$, $\bar{\chi} = 0{\cdot}87$ at the hinge line. (*b*) $M_\infty = 20$, $\alpha_{\text{wedge}} = 16°$, $\bar{\chi} = 19{\cdot}8$ at the hinge line. (*c*) $M_\infty = 20$, $\alpha_w = 21°$, $\bar{\chi} = 19{\cdot}8$ at the hinge line.

It is noticeable in many of the comparisons that the predictions 'lag' on the measurements in regions of strong pressure gradient. This may be due to the inability of the mathematical model to recognise either upstream influence or the presence of normal pressure gradients.

3.6. *Flow past expansion corners*

Both methods are applied to an expansion corner in figure 11 and both give predictions which are in reasonable agreement with the experimental data. The calculation using Sullivan's method is particularly good over the wedge-surface ahead of the corner. Both methods predict the rapid drop in pressure just downstream of the corner and the subsequent very slow decline towards the final level. The comparison further shows how in practice the influence of the

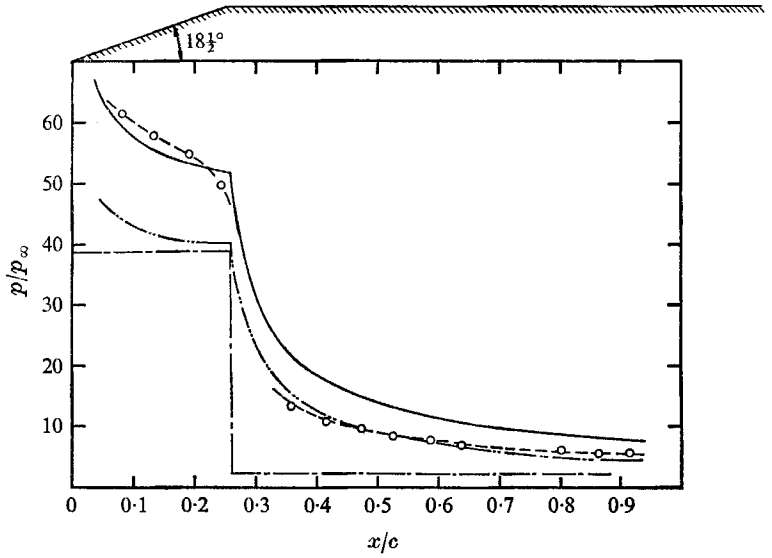

FIGURE 11. Pressure distribution over an expansion corner model at zero incidence—a comparison between theory and experiment. – – O – –, measurements, $M_\infty = 14{\cdot}8$, $\bar{\chi} = 18{\cdot}9$ at the corner. Theory: ——, Sullivan; — - - —, Cheng; — · —, inviscid.

corner feeds upstream, an effect which neither theory can predict, and how erroneous the inviscid pressure distribution is under these test conditions. Considering how non-similar the experimental profiles were downstream of the corner the predictions are surprisingly good.

4. Concluding remarks

Lees' 'local flat plate similarity' method for calculating boundary-layer growth can be combined with any one of a number of approximate pressure laws linking pressure to the slope of the effective body (body plus displacement thickness) to estimate the effect of viscous interaction on any two-dimensional surface with a sharp leading edge. If the Newton–Busemann law is used as Cheng did

then the results when oscillatory, greatly over-emphasise the experimental variations; however, the importance of the parameter $(M^2\alpha^2/A\bar{\chi})$ is immediately highlighted. If the tangent-wedge rule is employed (as Sullivan did to examine the flow downstream of an expansion) or the modified Newtonian rule is used, as in one of the examples here, then the results predict the main features of the flow very well.

The theory should be useful provided the boundary-layer profiles are reasonably similar. Its accuracy must decrease as separation conditions are approached and of course this technique can give no indication of either separation or upstream influence.

Comparisons between predictions and experimental data over a wide variety of conditions give some confidence in the use of the mathematical model for initial design purposes.

It is a pleasure to acknowledge the enthusiastic support provided by Mr D. Stevens of SRL who developed and ran the computer programs involved in this study.

REFERENCES

CHENG, H. K., HALL, J. G., GOLIAN, T. C. & HERTZBERG, A. 1961 'Boundary-layer displacement and leading-edge bluntness effects in high-temperature hypersonic flow'. *J. Aero. Sci.* **28**, 353.

CHENG, H. K. & KIRSCH, J. W. 1969 On the gas dynamics of an intense explosion with an expanding contact surface. *J. Fluid. Mech.* **39**, 289–305.

DEWEY, C. F. 1963 The use of local similarity concepts in hypersonic viscous interaction problems. *AIAA J.* **1**, 20.

HOLDEN, M. S. 1970 Boundary layer displacement and leading edge bluntness effects on attached and separated laminar boundary layers in a compression corner. Part II. Experimental studies. To be published.

KEMP, J. H. 1969 Hypersonic viscous interaction on sharp and blunt inclined plates. *AIAA J.* **7**, 1280.

LEES, L. 1956 Laminar heat transfer over blunt nosed bodies at hypersonic flight speeds. *Jet Propulsion*, **26**, 259.

SULLIVAN, P. A. 1969 On the interaction of a laminar hypersonic boundary layer and a corner expansion wave. *AIAA Paper* no. 69–137.

SULLIVAN, P. A. 1968 On the interaction of a laminar hypersonic boundary layer and a corner wave. *University of Toronto, UTIAS Tech. Note* 129.